TRENDS IN SCIENCES 2026; 23(1): 10715
https://doi.org/10.48048/tis.2026.10715 RESEARCH ARTICLE

Repositioning of Angiotensin II Receptor Blockers for Alzheimer's Disease: An *In-Silico* Study

Juan David Garcés-Barraza[1], Neyder Contreras-Puentes[2,*], Isabella Manzur-Villalobos[3], Antistio Alvíz-Amador[4], Janer Zabaleta-Guzmán[4] and Marlene Durán-Lenguas[5]

[1]*TOXSA, Medicine, Rafael Núñez University Corporation, Cartagena, Colombia*
[2]*GINUMED, Medicine, Rafael Núñez University Corporation, Cartagena, Colombia*
[3]*Departament of Pharmacology, University of Cartagena, Cartagena, Colombia*
[4]*Pharmacology and Therapeutics group, Pharmaceutical Chemistry Program, University of Cartagena, Cartagena, Colombia*
[5]*FARMABAC, Medicine Program, University of Cartagena, Cartagena, Colombia*

([*]Corresponding author's e-mail: neyder.contreras@campusuninunez.edu.co)

Received: 20 May 2025, Revised: 21 July 2025, Accepted: 28 July 2025, Published: 20 October 2025

Abstract

The brain renin-angiotensin-aldosterone system (RAAS), through angiotensin II and its AT1 and AT2 receptors, plays a pivotal role in blood pressure regulation and has been implicated in neurodegenerative processes such as Alzheimer's disease (AD). Angiotensin II receptor blockers (ARBs) inhibit the activation of AT1 receptors, thereby favoring an alternative RAAS pathway mediated by angiotensin IV (Ang-IV) and the AT4 receptor, providing protective effects for the nervous system. In this study, an *In-silico* evaluation of eight ARBs was performed by molecular docking (AutoDock Vina) and molecular dynamics simulations (AMBER20), assessing their binding affinity and conformational behavior with AT1 and AT2 receptors. Telmisartan and candesartan exhibited the highest affinity for AT1, with binding energies of −10.57 ± 0.12 and −9.83 ± 0.06 kcal/mol, respectively. For AT2, telmisartan showed a binding affinity of −10.60 ± 0.00 kcal/mol, although lower than the control ligand (−13.50 kcal/mol). Molecular dynamics simulations revealed that the AT1-telmisartan and AT1–candesartan complexes maintained structural stability with RMSD values remaining below 2.5 Å. The AT1–telmisartan complex exhibited the smallest radius of gyration (< 20 Å) and a reduced solvent accessible surface area (SASA), suggesting a compact and stable conformation. In contrast, the AT2–telmisartan complex demonstrated increased structural fluctuations (RMSF) within amino acid regions 60 - 75, 105 - 120 and 230 - 245, although overall stability was preserved throughout the 100 ns of simulation. These findings suggest that telmisartan and candesartan are promising candidates for modulating brain RAAS and could be considered as potential agents in Alzheimer's disease. Further *in vivo* validation is warranted to confirm their neuroprotective effect.

Keywords: Alzheimer's disease, Angiotensin II receptor blockers, Renin-angiotensin system, Molecular docking, Molecular dynamics simulation

Introduction

Angiotensin II receptor blockers (ARBs) exert beneficial effects by inhibiting the AT1 receptors of angiotensin II, inducing a decrease in vasoconstriction and fluid retention and therefore into cardiovascular improvements [1]. Additionally, some ARBs activate the nuclear receptor PPAR-γ, generating anti-inflammatory and antioxidant effects useful in diseases such as diabetes and cardiovascular disorders [2].

At the renal level, ARBs reduce proteinuria and slow the progression of chronic kidney disease, directly countering arteriolar vasoconstriction and aldosterone stimulation induced by angiotensin II [3]. In the central nervous system (CNS), shown to improve cognitive

function and exert neuroprotective effects in Alzheimer's disease (AD), which is attributed to their action on the brain renin-angiotensin system, particularly in the aminopeptidase/Ang IV/AT4 receptor axis [4,5]. This activation of the alternative axis reduces reactive oxygen species and microglial activation, promoting an anti-inflammatory environment in the CNS [6].

Likewise, through the circumventricular organs (CVO), the peripheral system allows the passage of components of the RAAS to the brain, while the central pathway connects the hypothalamus with the medulla oblongata through structures such as the area postrema (AP) and the solitary tract nuclei (NST), responsible for the local production of angiotensin [4,7,8]. The activity of the brain RAS is also involved in neuronal plasticity, the control of oxidative stress, and neurogenic inflammation [9].

The AT1 receptor favored inflammatory and oxidative processes; its inhibition promoted the conversion of Ang II to Ang IV, improving cognition in animal models [3]. The AT4 receptor, activated by Ang IV, has been shown to restore spatial memory, improve cerebral flow and promote neuroprotection [5,10]. On the other hand, the AT2 receptor, present in the adult brain, acts on a non-classical pathway that generates Ang (1–7) through the action of ACE2, which exerts protective effects via the Mas receptor. Additionally, the brain also contains angiotensin III and IV. The neuronal isoform renin-b, for its part, antagonizes the effects of renin-a, contributing to a neuroprotective effect of the cerebral RAS [11].

ARBs such as losartan, candesartan and telmisartan are studied in Alzheimer's disease, given that hypertension is a vascular risk factor for this neurodegenerative disease [12]. The brain RAAS contains the necessary elements for active central function and the binding of Ang II to the AT1 and AT2 receptors, including active peptide Ang IV to the AT4 receptor, are associated with vascular, neuronal and cognitive effects [3,13]. ARBs can treat mild cognitive impairment, delay cognitive decline in Alzheimer's patients and prevent cerebrovascular dysfunction and accumulation of beta-amyloid proteins [10,14]. The pharmacokinetic characteristics of some ARBs, mainly candesartan and telmisartan, favor their activity at a central level due to their ability to cross the blood-brain barrier [15].

Therefore, with the advancement of technology, *In silico* studies have been promoted as deeper tools for the explanation of potential mechanisms. Methodologies such as molecular docking, structure-activity relationship (SAR), pharmacophore modeling and molecular dynamics simulations have emerged as complementary approaches that enable the prediction of novel therapeutic targets, the optimization of drug candidates and preliminary exploration of possible molecular pathways implicated in pathologies such as Alzheimer's disease [16].

The objective is to allow the *In silico* evaluation of drugs such as ARBs against AT1 and AT2 receptors, linking their direct activity to the local brain Renin-Angiotensin-Aldosterone System (RAAS), performing a predictive analysis and conducting receptor affinity and conformational studies.

Materials and methods

Preparation of receptors

A preliminary search for potential crystal structures for molecular docking was conducted. These crystals were selected according to optimal resolution, adequate validation (Ligand Structure Quality Assessment) and the presence of co-crystallized ligands that allow validation of the docking. Thus, a search was performed for Type 1 and 2 angiotensin II receptors in UniProt (P30556 - AGTR1_HUMAN and P50052 - AGTR2_HUMAN), where 6 and 7 structures were identified, respectively (See Supplementary Material **Tables S1** and **S2**).

The protein structures of the angiotensin II receptors as AT1 and AT2 were obtained through the Protein Data Bank (PDB) database, identified with the codes 4ZUD (resolution: 2.80 Å) and 5UNF (resolution: 2.80 Å), respectively. Previously, the crystals were evaluated for missing residues and completed using pdb4AMBER, continuing with the observation of the viability of the structures through the Ramachandran plot, using RampPlot [17]. (Supplementary Material - **Figures S1** - **S8**)

Subsequently, the crystal structures were prepared using AutoDock Tools (ADT; v.1.5.6) [18], following the stages of removing water molecules and additional ligands, incorporating hydrogens, adding Kollman

charges and fusion of non-polar hydrogens. Finally, it was saved in pdbqt format for the development of molecular docking.

Ligand selection and preparation

Based on previously published experimental studies regarding the hypothetical role of ARBs as candidates in the treatment of Alzheimer's disease, 8 molecules were selected and downloaded in sdf format using the PubChem database. Next, the proteins were geometrically optimized using the Gaussian 09W software, applying the theoretical DFT(B3LYP)/6-31+G(d) optimization method, to obtain a stable energy conformation before molecular docking.

Each molecule once optimized was saved in mol2 format, then prepared using AutoDock Tools with the addition of hydrogens, Gasteiger charges and removal of non-polar hydrogens; Finally, each structure was converted into pdbqt format through Open Babel tools v2.3, with the --gen3d parameter enabled and default settings [19].

Molecular docking

The selection of boxes location and size of the boxes was guided by the position of key residues identified in co-crystallized structures and in previous studies. The optimal conformation of each complex was determined based on the lowest binding energy and root-mean-square deviation (RMSD) ≤ 2.0 Å relative to the reference pose. Automatic clustering was not applied.

Each molecular docking run was executed in triplicate using AutoDock-Vina v.1.1.2 [20]. For this, a grid spacing of x = –40.989 Å x y = 63.050 Å x z = 20.015 Å for AT1 and x = 80.966 Å x y = -3.189 Å x z = 36.769 Å for AT2 was used, respectively. Additionally, the dimensions of the boxes were x = 16.823 Å x y = 13.67 Å x z = 14.20 Å for AT1 and x = 18.46 Å x y = 18.22 Å x z = 20.36 Å for AT2. The best poses for each system were considered and the energy affinity values were expressed in terms of kcal/mol ± standard deviation (SD). The interactions between the complexes obtained were visualized using the Discovery Studio Visualizer program v.21.1 [21].

Molecular dynamics simulation

The complexes for AT1 and AT2 with the best energy score and reference molecules were subjected to molecular dynamics (MD) simulations. Unconstrained MD simulations were performed for all atoms using AMBER20 software. The minimization, equilibrium and production procedures were developed according to the protocol of Alviz-Amador *et al.* [22]. The ff14SB and GAFF2 force fields were applied to the respective receptors and ligands.

TIP3P water-solvated structures were subjected to minimization that included 1,000 steep descent steps, continuing with 1,000 conjugate gradient minimization steps. Additionally, a constant force constraint of 25 kcal/mol-Å^2 was applied. Next, a heating process was executed using 5,000 steps from 100 K to 300 K, with time intervals of 2 femtoseconds (fs). During this heating, a loosely coupled thermostat was used at constant pressure and bonds involving hydrogen were constrained using the SHAKE algorithm, with a tolerance set to 0.00001. Interactions were established at a non-bonded cutoff radius of 8 Å.

Subsequently, the restrictions applied to peptides and proteins were gradually reduced from 5 to 0.5 kcal/mol-Å2 in five steps. An initial minimization was performed with 1,000 steps descent steps, followed by 500 steps of conjugate gradient minimization, using a time of 2 femtoseconds (fs). Then, a 50 picoseconds (ps) molecular dynamics simulation was carried out at 300 K, with constant pressure and temperature using Berendsen constants of 0.2 ps. The stability of the system during the equilibrium phase was confirmed by monitoring the temperature and pressure curves. The total simulation time is 100 ns.

Subsequently, root mean square deviation (RMSD) analysis, mobility analysis using root mean square fluctuation (RMSF), radius of gyration (Rg) measurement and solvent accessible surface area (SASA) were performed. The analyses were executed using the CPPTRAJ program [23].

Binding free energy calculations

The MM-GBSA method was used with the MMPBSA.py tool to determine the binding affinity of different ligands to the receptor [24]. A total of 100 ns were extracted from the molecular dynamic's simulation and the ΔG_{Total} was calculated following the methodology developed by Alviz-Amador *et al*. [22]. Calculating the free energy (ΔG), the protein's entropic contribution was excluded because the binding energy

was used to determine the relative binding strength of each complex without considering the effect of entropy in the calculation. The analysis focused on relative comparisons between complexes. Energy efficiency per residue was not assessed.

Results and discussion

Research shows that the brain's renin-angiotensin-aldosterone system (RAAS) is linked to the development of Alzheimer's disease (AD), making it a hopeful target for finding effective treatments for this brain disorder. Over the years and with multiple investigations worldwide, angiotensin II receptor inhibitors (ARBs) have emerged as a relevant therapeutic option for patients affected by this pathology.

Preclinical and clinical studies support the efficacy of ARBs in Alzheimer's disease (AD). Danielyan *et al*. found that losartan greatly lowered the buildup of beta-amyloid plaques and helped improve thinking skills in mice with Alzheimer's disease [25]. Deng *et al*. suggested that ARBs are associated with a lower risk of dementia compared to other antihypertensive drugs [26]. Similarly, the positive effects of ARBs on brain inflammation were emphasized, strengthening the proof of their protective benefits for the brain [27]. Ongali *et al*. Ongali *et al*. demonstrated that losartan prevents and reverses cerebrovascular, neuropathological and cognitive deficits associated with AD [28].

Subsequent studies examined different ARBs in animal models of AD, suggesting these drugs reduce the accumulation of β-amyloid plaques and significantly improve cognitive function [29-31]. Alike, it has been revealed that candesartan can protect against brain disorders associated with aging and senescence [32]. The latest findings highlight the ability of candesartan to protect against D-galactose-induced neurotoxicity and memory deficits through modulation of autophagy and oxidative stress, suggesting its potential as a promising candidate for age-related neurodegenerative disorders and memory deficits [33].

Clinical studies and meta-analysis have evidenced that patients treated with ARBs exhibit a decreased risk of Alzheimer's disease relative to other antihypertensive medications (RR = 0.78, 95% CI 0.68 - 0.88; *p-value* < 0.001) [34]. Similarly, ARBs may diminish the risk of Alzheimer's disease, maybe through supplementary neuroprotective mechanisms outside blood pressure regulation [35]. In contrast, Medications that stimulate AT2/AT4 receptors had a lower association with dementia compared to inhibitors such as ACE inhibitors [36].

The studies provide robust evidence of therapeutic benefits of ARBs, especially Candesartan and Telmisartan, in Alzheimer's disease (AD), through diverse mechanisms including anti-inflammatory action and enhancement of cerebrovascular integrity. These results support the consideration of ARBs as valuable therapeutic options in AD and underline the need for future research to completely understand their mechanisms of action and optimize their clinical application.

Molecular docking

Eight ligands corresponding to ARB drugs with AT1 and AT2 receptors were evaluated and the ligand with the highest affinity for each receptor type was determined (Supplementary Material - **Figures S9** and **S10**). For the molecular docking, it was observed that two ligands, telmisartan and candesartan, exhibited a greater affinity with the AT1 receptor compared to the reference ligand, with binding energies of –10.57 ± 0.12 and –9.83 ± 0.06 kcal/mol, respectively, compared to the energy of the reference ligand binding at –9.50 ± 0.00 kcal/mol. These results suggest that both molecules have an enhanced affinity for the AT1 receptor. (See **Table 1** and **Figure 1**).

Table 1 Main ARBs that interact with AT1 and AT2 receptors.

Protein	Ligand	Binding energy (kcal/mol ± SD)	Hydrophobic interaction	H-bond interaction
AT1 receptor	Telmisartan*	–10.57 ± 0.12	Y35, F77, Y108, S109, A181, I288, Y292, Y293, W253	R167

Protein	Ligand	Binding energy (kcal/mol ± SD)	Hydrophobic interaction	H-bond interaction
	Candesartan*	–9.83 ± 0.06	W84, V108, A181, M234, I288	Y35
	Azilsartan	–9.47 ± 0.12	W84, V108, L112, K199, W253, I288, Y292	R167
	Ibersartan	–9.40 ± 0.00	Y35, W84, Y92, V108, W253, I288, M284	T88
	Olmesartan	–9.00 ± 0.00	Y35, W84, Y87, Y92, V108, R167, W253, I288, M284	T88
	Losartan	–8.77 ± 0.06	W84, V108, R167, Y184, M284, I288	Y35, F182
	Eprosartan	–8.50 ± 0.00	Y35, F77, W84, Y87, Y92, V108, R167, I288	167
	Valsartan	–8.27 ± 0.15	Y35, W84, Y87, Y92, V108, R167	-
	OLM[a]	–9.50 ± 0.00	W84, Y87, Y92, Y108, R167, H256, M284, P285, Y292	Y35, T88
AT2 receptor	Telmisartan*	–10.60 ± 0.00	L93, W100, L124, R182, M214, F272, I304, F308	K215
	Ibersartan	–10.03 ± 0.12	W100, L124, T125, M128, I304, F308	T125, R182
	Azilsartan	–9.47 ± 0,45	W100, L124, T125, M128, R182, M197, M214, K215, W269, I304, F308	T125, R182
	Olmesartan	–9.37 ± 0.06	W100, Y104, Y108, L124, T125, M128, R182, F272, I304	C195, K215
	Eprosartan	–8.93 ± 0.06	L93, L124, M128, K215, W269, L300, I304, F308	W100, R182
	Losartan	–8.87 ± 0.06	Y51, W100, Y108, L124, M128, I304	Y103, C195, K215
	Candesartan*	–8.70 ± 0.17	L93, W100, T178, M214, K215, I304	T125, R182
	Valsartan	–8.23 ± 0.21	W100, Y103, L124, I304, F308	T125, R182
	8ES	–13.50 ± 0.00	W100, Y108, T125, R182, C195, W209, M214, K215, I304, F308	L124, T178

aCocrystalized ligand AT1 receptor; bCocrystalized ligand AT2 receptor; *ARBs that crosses the BBB

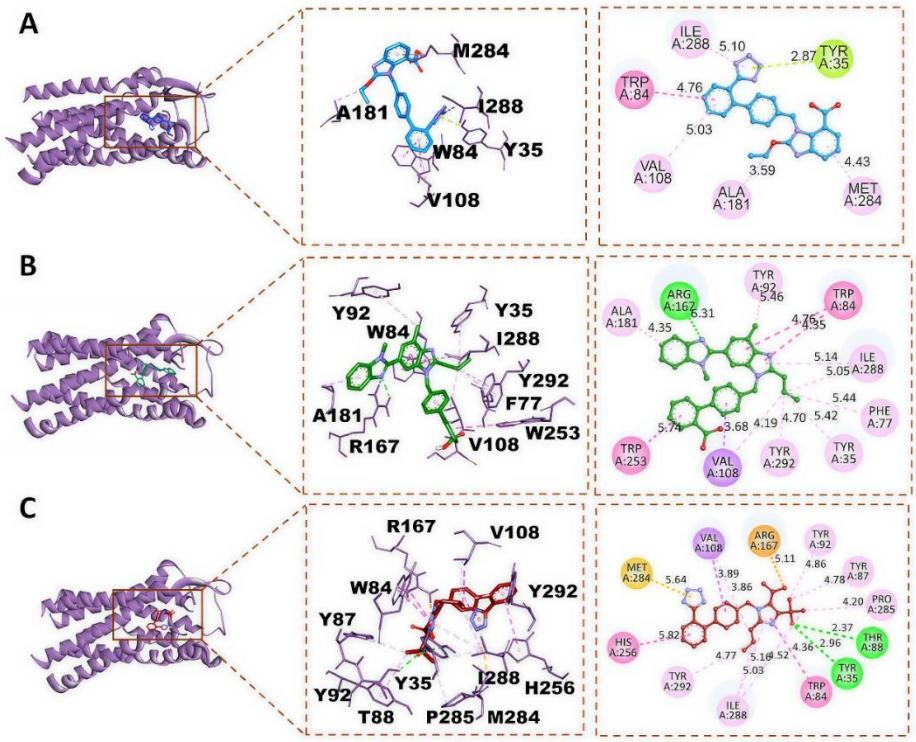

Figure 1 Important interactions between reference inhibitors and ARBs against AT1 receptor. A. Telmisartan; B. Candesartan; C. OLM: Selective inhibitor of AT1 receptor.

A critical residue in the docking of these three ligands is Tyr35$^{(1.39\ Å)}$, evidencing a hydrogen bond between this residue and the imidazole group of ligands. These findings support the research of Zhang *et al*., who pointed out that this hydrogen bond is crucial for the stability and specificity of the binding of the ligand to the receptor pocket, a fundamental aspect for the pharmacological activity of AT1 receptor antagonists such as olmesartan, candesartan and telmisartan [37].

In the molecular docking analysis of AT1 receptor, it has been reported that the tetrazole ring of candesartan can form both salt bridge and H-bond interactions with Arg167 (ECL2), while the carboxyl group is oriented toward Lys199 [38]. Additionally, the biphenyl structure of candesartan engages in aromatic interactions with Trp84, which in turn can generate stabilization through a hydrogen bond with Tyr35. Furthermore, residues such as Val108, Met284 and I288 enhance ligand anchoring within the binding pocket. Similarly, telmisartan has been shown to form an H-bond with Arg167 and together with Lys199 can establish a bidentate interaction with the positively charged residues in the binding pocket site [39].

It has been suggested that Tyr92 in ECL1 plays a key role in π-π stacking interactions at the pocket entrance, critically influencing ligand affinity. Aromatic residues such as Trp253, located in helix VI, further reinforce binding through hydrophobic and π-π interactions. Regarding the OLM analogue, the ligand is positioned within the binding pocket, where the carbamoyl group interacts with H-bonds of helix II, including Thr88 and Tyr35. Similarly, studies show that Tyr35 interacts with OLM analogues through binding to Tyr87/Thr88. Similarly, it has been observed that His256 and Pro285 promote ligand interaction, whereas residues such as Val108, Ile288 and Tyr292 enhance hydrophobic core binding, which are consistent of the findings in the research [37-40].

The evaluation of AT2 receptor identified specific residues, such as Arg182, Thr125 and Thr178, located in the ligand binding pocket region, which plays a crucial role in interactions with the AT2 receptor [41]. It has been indicated that neither telmisartan nor candesartan presented a higher affinity than the reference ligand 8ES, which exhibited a binding energy of –13.50 ± 0.00 kcal/mol. It is crucial to note that telmisartan demonstrated a considerably better affinity,

with binding energies of –10.60 ± 0.00 kcal/mol, compared to those recorded for candesartan, which was –8.70 ± 0.17 kcal/mol. All three residues are critical in docking the ligands (Candesartan, telmisartan and the reference ligand 8ES) with the AT2 receptor (See **Table 1** and **Figure 2**). Both Arg182, Thr125 and Thr178 form a hydrogen bond with the tetrazole ring of the ligands [41]. These critical interactions for selective ligand binding to AT2 contribute to the diversity of ligand binding between the two types of angiotensin II receptors.

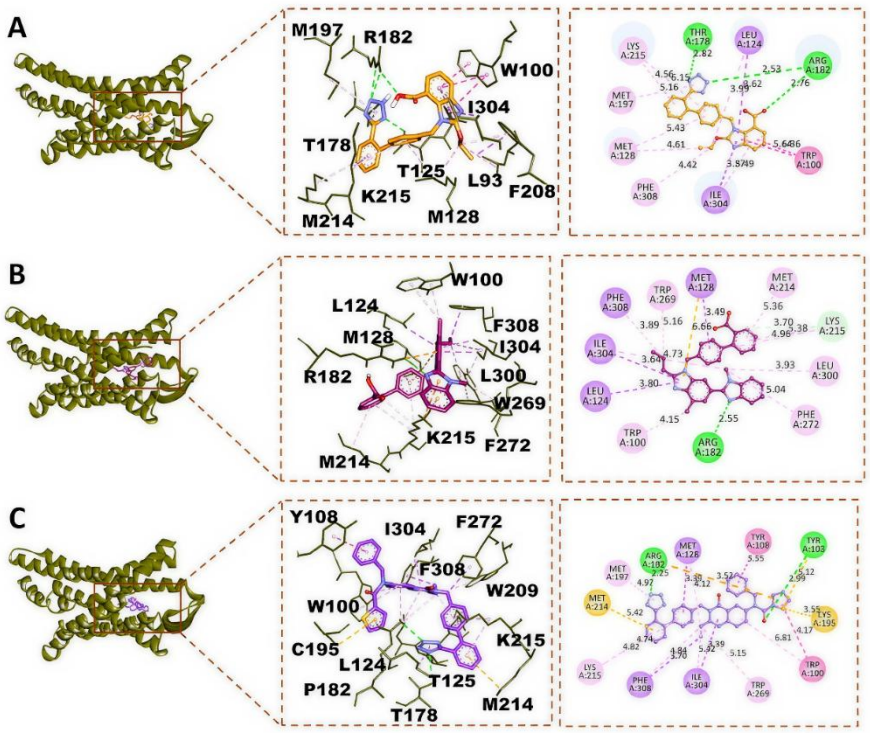

Figure 2 Important interactions between reference inhibitors and ARBs against AT2 receptors. A. Telmisartan; B. Candesartan; C. 8ES: Selective inhibitor of AT2 receptor.

Furthermore, the mutation of Arg182 to Ala182 has been shown to significantly reduce ligand affinity and activation of intracellular signaling, indicating that Arg182 is important for receptor function. It has been demonstrated that the tetrazole ring in both candesartan and the co-crystallized analogue interacts with Arg182 (ECL2) through hydrogen bonding, as previously reported in other studies. These interactions have been associated with ligand anchoring and enhanced binding affinity. In contrast, Arg182 with telmisartan primarily forms an H-bond with the carboxylate group of the ligand. Similarly, the carboxylate moiety of telmisartan established a strong salt bridge with Lys215, which may facilitate the anchoring of telmisartan analogues [42]. At the level of the hydrophobic contour of the AT2 receptor, candesartan interacts with Trp100 and Met214, which contribute to structural compaction. Unlike earlier studies that describe interactions with the biphenyl ring, Trp100 in this context appears to interact with the benzimidazole moiety [43].

For the telmisartan-AT2 receptor complex, contacts are distinguished between biphenyl and benzimidazole rings and extended residues such as Leu93, Trp100, Met214, Ile304; Furthermore, interactions with Phe272 and Phe308, with the latter perhaps penetrating more into the receptor binding pocket, which may explain variations in binding affinity. Moreover, the structure of the co-crystallized analogue extends toward Tyr108 and Cys195 near the pocket entrance. A carbonyl group of the quinazolinone core forms an H-bond with Tyr108 (helix III), contributing to ligand stabilization. Meanwhile, Cys195 remains close, participating in the van der Waals

interactions that influence ligand closure within the binding site [42].

Molecular dynamics

In the AT1 systems, structural folding, as indicated by the RMSD values, remained moderately fluctuating in the first 50 ns of simulation. The RMSD of the inhibitory ligands linked to AT1 exhibited improved structural stability, reaching values less than 2 Å after 50 ns, maintaining proper folding based in the criteria by Deng *et al*. [44] (**Figure 3(A)**). Additionally, AT1-native, AT1-telmisartan and AT1-Cocrystal generally maintain greater stability throughout the simulation, reaching values lower than 2.5 Å.

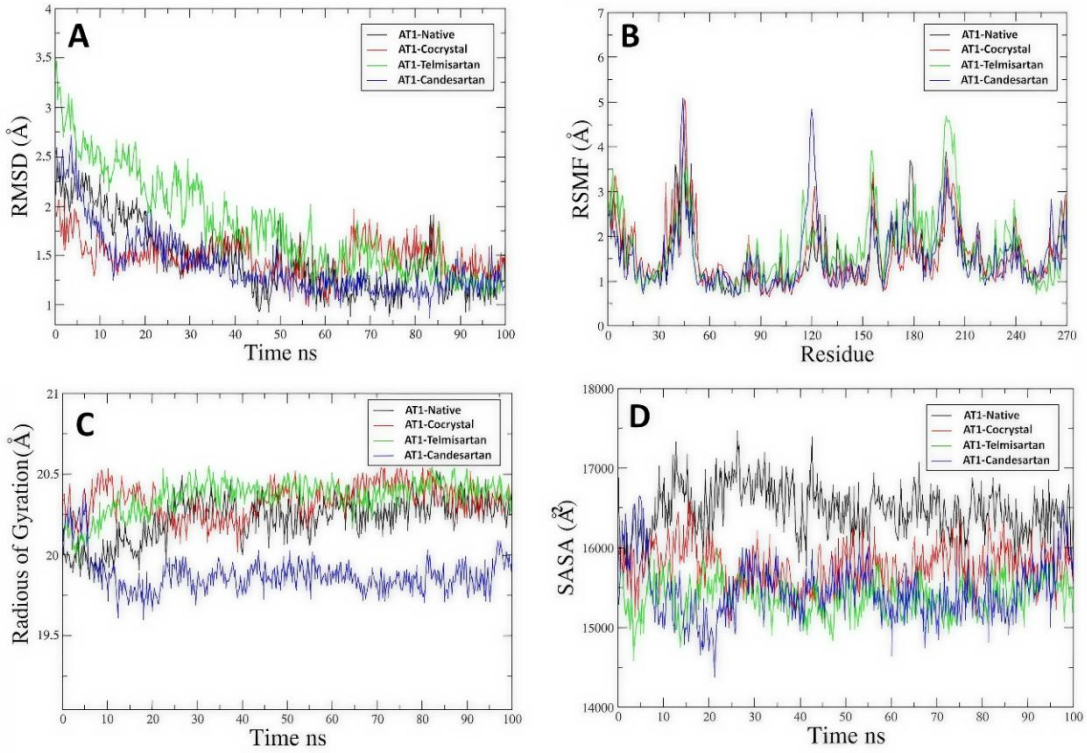

Figure 3 Molecular dynamics analysis of co-crystallized candesartan, telmisartan and inhibitor bound to the AT1 receptor. A. Root Mean Square (RMSD). B. Root means square fluctuation (RMSF). C. Radius of gyration (RoG). D. Solvent-accessible surface area (SASA).

Regarding the RMSF results, AT1-Telmisartan demonstrated increased flexibility in the region spanning residues 100 to 135 aa, with greater fluctuation compared to other systems (**Figure 3(B)**); likewise, AT1-Candesartan complex exhibited elevated mobility between 195 to 210 aa. It has been reported that local flexibility on the receptor can influence ligand interactions; specifically, telmisartan binding to AT1 does not maintain complete rigidity in the ECL1 loop around of TM3, resulting in increased flexibility in this region. Residues such as Ser105 and Ser109 (TM3), are stabilized via hydrogen bonding with ARBs containing tetrazole rings [45].

On the other hand, it has been observed that telmisartan, compared to candesartan, has a less intense interaction with Tyr92 (ECL1). Moreover, in certain studies, the mutation of Tyr by Ala results in a decrease in the affinity of telmisartan, suggesting that its contribution to binding is indirect, as well as to the stabilization of Arg167. Therefore, the ECL1 loop remains slightly more flexible with telmisartan compared to other ligands [37].

Only the AT1-Candesartan system initially presents 3 Å records that subsequently reach stability. The RMSF indicated mobilities in the amino acid sequences between CLSIDRYLAIVHPTMLVAKVT for the AT1-Telmisartan system where it reached values of 5 Å for the other systems. Similarly, a pronounced fluctuation is present in the AT1-Candesartan system, associated explicitly with the TLIWKALNDDIFKIIM

sequence. However, it is not directly related to the area of the residues involved in catalysis, indicating possible structural changes or mobilities with candesartan. However, when relating key residues in interaction, such as Arg167, it has been shown that in the area close to the amino acid, slight changes in mobility are observed for the other systems evaluated, which tend to be more conserved than the native protein [37].

Regarding the radius of gyration (Rg), lower values were evident for AT1-Telmisartan, showing values lower than 20 Å in comparison to other systems (**Figure 3(C)**). The AT1-Telmisartan system was identified to present greater compactness in contrast to all the systems by showing a lower value, which may be associated with the presence of interactions and factors such as the spatial distribution of the ligands in the protein, the number and type of contacts per residue, which are modifiers independent of the size of the protein [46]. For the behavior of SASA in AT1, it was evidenced that ARBs and the co-crystallized molecule presented a similar behavior when compared to the native protein, with lower values being recorded in AT1-Telmisartan and AT1-Candesartan (**Figure 3(D)**). The SASA values demonstrated that the inhibitors, including Telmisartan, showed a tendency to generate restricted accessibility, which indicates a certain degree of considerable affinity on the binding site, resulting in an indicator of stability to the receptor.

In the molecular dynamics simulations for AT2, it was shown that the RSMD values were usually below 3 Å, with more significant changes seen with AT2-Telmisartan, which had values over 2 Å compared to the original protein (**Figure 4(A)**). The results show a better folding profile and structural stability for the latter two, due to maintaining RSMD value averages lower than 2 Å. However, although the AT2-telmisartan system showed higher values, it maintained considerable stability according to what was outlined by Deng *et al*. [44]. In the AT2 systems, the molecule that showed the biggest changes was AT2-telmisartan, which had many ups and downs in the regions between amino acid residues 60 - 75, 105 - 120, 135 - 150 and 230 - 245 (**Figure 4(B)**).

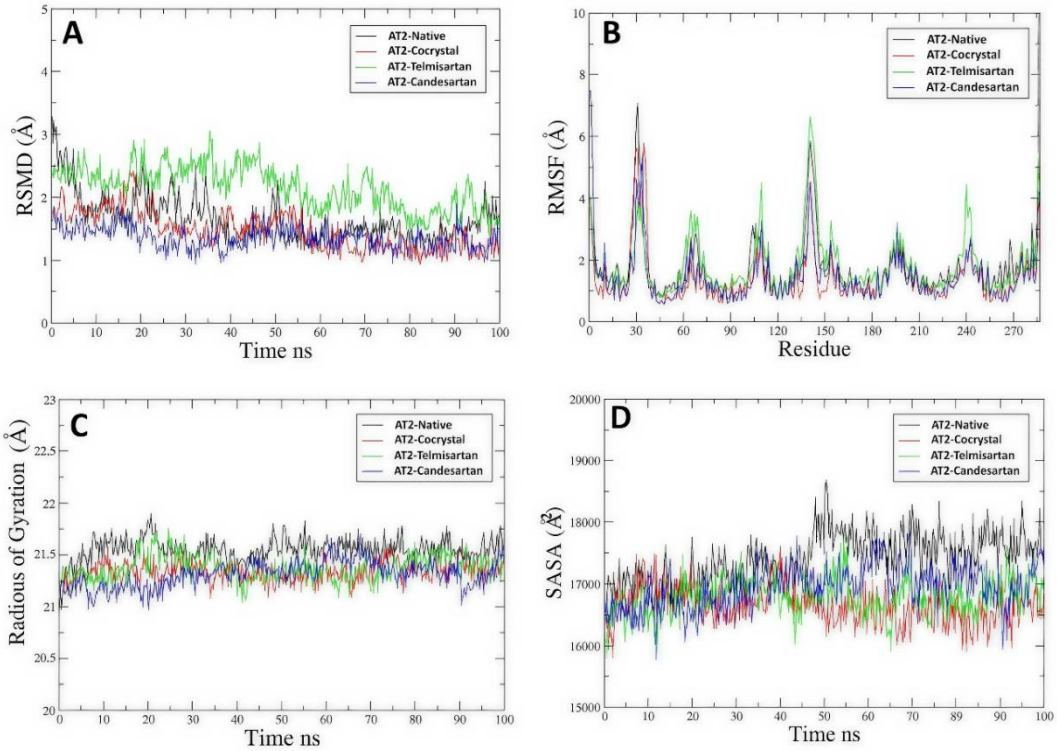

Figure 4 Molecular dynamics analysis of co-crystallized candesartan, telmisartan and inhibitor bound to AT2 receptor. A. Root Mean Square (RMSD). B. Root means square fluctuation (RMSF). C. Radius of gyration (RoG). D. Solvent-accessible surface area (SASA).

RMSF only showed notable variations with AT2-telmisartan in sequences such as TYYSYRYDWLFGPVMC, where key catalytic site residues such as Trp100 and Tyr104 are identified, which may present interaction with aromatic groups of ARBs [41]. On the other hand, variations have been described in areas of amino acid residues between WMGVINSCEVI and even though fluctuations occur in these regions, key residues in the activity of the receptor are not shown. Regarding the behavior of the radius of gyration, minimal variations were evidenced between all the studied simulations; however, for the three inhibitors evaluated, a lower value was noted throughout the entire simulation when compared with the AT2-Native system (**Figure 4(C)**). Similarly, the SASA values in AT2 were similar in the ARB and Co-crystallized drugs, which fluctuated to a lesser extent and even from 50 ns onwards when contrasted with AT2 without the presence of ligands (**Figure 4(D)**).

The MMGBSA method was used to calculate the binding free energy results, as shown in **Table 2**. The table presents the components that contribute to the binding free energy of the AT1 and AT2 receptor complexes with ARB analogs and controls. Notably, the total value of the binding free energy (ΔG_{TOTAL}) in all systems obtained was negative, suggesting a favorable binding interaction. However, AT1-Telmisartan showed a higher energy value than AT1-Candesartan and AT1-control, coinciding with the results obtained by molecular docking. Likewise, it was evidenced that AT2-Control presented the highest activity, followed by AT2-Telmisartan, with a better energy score than AT2-Candesartan.

Table 2 Binding free energy components (kcal/mol) of AT1 and AT2 receptors and ARBs and control by MMGBSA method.

Energy component	VDW	EEL	EGB	ESURF	ΔG_{gas}	ΔG_{solv}	ΔG_{Total} ± SD (kcal/mol)
AT1-Telmisartan	–69.32	–4.83	16.03	–7.49	–74.15	8.55	–65.69
AT1-Candesartan	–63.12	–28.99	41.49	–6.91	–92.12	34.59	–57.53
AT1-Control (OLM)	–12.22	–88.23	39.53	–2.28	–45.63	37.25	−8.38
AT2-Telmisartan	–60.95	55.06	-43.78	–6.89	–5.90	–50.67	–56.56
AT2-Candesartan	–51.81	–14.90	28.69	–5.66	–66.71	23.02	–43.69
AT2-Control (ES8)	–79.92	53.45	–34.72	–8.84	–26.48	–43.56	–70.04

EEL: Electrostatic energy, EGB: Summation of electrostatic, ESURF: Surface energy, ΔG gas: Gibb's energy in the gas phase ΔG sol: Gibb´s energy in aqueous phase, ΔG Total: Total Gibb´s energy, VDW: Van der Waals.

The ΔG_{Total} values obtained by MMGBSA were negative for all complexes, indicating a thermodynamically favorable interaction. AT1-candesartan showed a more favorable ΔGTotal than AT1-telmisartan, consistent with its more stable hydrophobic interaction profile. In AT2, although the control was superior, telmisartan outperformed candesartan in ΔGTotal. These findings suggest that affinity depends not only on the total free energy but also on the distribution of specific interactions and the structural stability of the complex. Electrostatic energy and van der Waals interactions were determinants of the ligand's greater affinity for AT1. In AT2, the data highlights the functional role of residues such as Arg182 and Trp100 in the effective binding of telmisartan.

Conclusions

This *in silico* study indicates that ARBs, particularly telmisartan and candesartan, due to their capacity to traverse the blood-brain barrier, demonstrate a strong affinity for AT1 and AT2 receptors, potentially elucidating their modulatory effects on the brain renin-angiotensin system, which is involved in the pathophysiology of Alzheimer's disease. Molecular docking revealed significant interactions of telmisartan and candesartan with the AT1 and AT2 receptors; specifically, Arg167, Tyr35 and Trp84 were identified for AT1, which are crucial for the ligands' affinity and inhibitory efficacy. In the AT2 receptors, Trp100, Thr125, Arg182 and Met214 were identified as contributors to the anchoring process and selectivity of ARBs, characterized by their binding capability through

polar and hydrophobic contacts, indicating diversity in affinity throughout the receptor. Molecular dynamics simulations, conversely, validated the structural stability of the complexes by the overall behaviour of RMSD, RMSF, SASA and RoG, with analogous trends in free energy, therefore corroborating the findings from molecular docking. Thus, it is confirmed that research will persist in substantiating the idea of the potential of these medicines for therapeutic repositioning in neurodegenerative disorders, including Alzheimer's Disease. Subsequent *in vivo* investigations and pharmacodynamic trials will be essential to corroborate these findings and progress towards clinical applications.

Acknowledgements

We thank the members of the Pharmacology and Therapeutics research group. As well as the members of the GINUMED of the Rafael Núñez University Corporation, Colombia.

Declaration of Generative AI in Scientific Writing

The authors are grateful for the use of generative AI tools, such as QuillBot, to correct grammatical errors in certain paragraphs of the manuscript. The authors did not use these tools to interpret the results or draw conclusions.

CRediT Author Statement

Juan Garcés-Barraza: Conceptualization, Methodology, Supervision, Validation, and Writing original draf. **Neyder Contreras-Puentes:** Conceptualization, Methodology, Supervision, Validation, and Writing original draf. **Isabella Manzur-Villalobos:** Formal analysis, Investigation, Validation, and Visualization. **Antistio Alviz-Amador:** Methodology, Formal analysis, Investigation, and Validation. **Janer Zabaleta-Guzmán:** Data curation, Formal analysis, and Visualization. **Marlene Durán-Lengua:** Project administration, Investigation, Supervision, Validation.

References

[1] CP Walther, WC Winkelmayer, PA Richardson, SS Virani and SD Navaneethan. Renin-angiotensin system blocker discontinuation and adverse outcomes in chronic kidney disease. *Nephrology Dialysis Transplantation* 2021; **36(10)**, 1893-1899.

[2] E Cantero-Navarro, B Fernández-Fernández, AM Ramos, S Rayego-Mateos, RR Rodrigues-Diez, MD Sánchez-Niño, AB Sanz, M Ruiz-Ortega and A Ortiz. Renin-angiotensin system and inflammation update. *Molecular and Cellular Endocrinology* 2021; **529**,111254.

[3] H Wu, Q Sun, S Yuan, J Wang, F Li, H Gao, X Chen, R Yang and J Xu. AT1 Receptors: Their actions from hypertension to cognitive impairment. *Cardiovascular Toxicology* 2022; **22(4)**, 311-325.

[4] F Gouveia, A Camins, M Ettcheto, J Bicker, A Falcão, MT Cruz and A Fortuna. Targeting brain Renin-Angiotensin system for the prevention and treatment of Alzheimer's disease. *Ageing research reviews* 2022; **77**, 101612.

[5] LJ Trigiani, J Royea, M Lacalle-Aurioles, XK Tong and E Hamel. Pleiotropic benefits of the angiotensin receptor blocker candesartan in a mouse model of Alzheimer disease. *Hypertension* 2018; **72(5)**, 1217-1226.

[6] M Molina-Van de Bosch, C Jacobs-Cachá, A Vergara, D Serón and MJ Soler. The renin-angiotensin system and the brain. *Hipertensión y Riesgo Vascular* 2021; **38(3)**, 125-132.

[7] VT Ribeiro, LC de Souza, AC Simões and E Silva. Renin-Angiotensin system and Alzheimer's disease pathophysiology: From the potential interactions to therapeutic perspectives. *Protein and Peptide Letters* 2020; **27(6)**, 484-511.

[8] CM Ferrario and AE Mullick. Renin angiotensin aldosterone inhibition in the treatment of cardiovascular disease. *Pharmacological Research* 2017; **125**, 57-71.

[9] OA Abiodun and MS Ola. Role of brain renin angiotensin system in neurodegeneration: An update. *Saudi Journal of Biological Sciences* 2020; **27(3)**, 905-912.

[10] CE Evans, JS Miners, G Piva, CL Willis, DM Heard, EJ Kidd, MA Good and PG Kehoe. ACE2 activation protects against cognitive decline and reduces amyloid pathology. *Acta Neuropathologica* 2020; **139(3)**, 485-502.

[11] J Royea and E Hamel. Brain angiotensin II and angiotensin IV receptors as potential Alzheimer's

disease therapeutic targets. *GeroScience* 2020; **42(5)**, 1237-1256.

[12] E Trofimiuk, P Wielgat and JJ Braszko. Candesartan, angiotensin II type 1 receptor blocker is able to relieve age-related cognitive impairment. *Pharmacological Reports* 2018; **70(1)**, 87-92.

[13] J Kulisevsky, S Martínez-Horta, A Campolongo, B Pascual-Sedano, J Marín-Lahoz, H Bejr-Kasem, JL Labandeira-Garcia, JL Lanciego, A Puig-Davi, A Horta-Barba, J Pagonabarraga and J Rodríguez-Antigüedad. A randomized clinical trial of candesartan for cognitive impairment in Parkinson's disease. *Parkinsonism & Related Disorders* 2023; **110**, 105367.

[14] PG Kehoe, S Wong, NA Mulhim, LE Palmer and JS Miners. Angiotensin-converting enzyme 2 is reduced in Alzheimer's disease. *Alzheimer's Research & Therapy* 2016; **8(1)**, 50.

[15] AG Elkahloun and JM Saavedra. Candesartan neuroprotection in rat primary neurons negatively correlates with aging and senescence: A transcriptomic analysis. *Molecular Neurobiology* 2020; **57(3)**, 1656-1673.

[16] B Shaker, S Ahmad, J Lee, C Jung and D Na. *In silico* methods and tools for drug discovery. *Computers in Biology and Medicine* 2021; **137**, 104851.

[17] M Kumar and RS Rathore. RamPlot: A webserver to draw 2D, 3D and assorted Ramachandran (φ, ψ) maps. *Journal of Applied Crystallography* 2025; **58(2)**, 630-636.

[18] GM Morris, H Ruth, W Lindstrom, MF Sanner, RK Belew, DS Goodsell and AJ Olson. AutoDock4 and AutoDockTools4: Automated docking. *Journal of Computational Chemistry* 2009; **30(16)**, 2785-2791.

[19] NM O'Boyle, M Banck, CA James, C Morley, T Vandermeersch and GR Hutchison. Open babel: An open chemical toolbox. *Journal of Cheminformatics* 2011; **3**, 33.

[20] O Trott and AJ Olson. Autodock vina: Improving speed and accuracy. *Journal of Computational Chemistry* 2010; **31(2)**, 455-461.

[21] E Bursal, MA Yılmaz, A Aras, F Türkan, Ü Yildiko, Ö Kılıç and A Dey. Determination of phenolic content, biological activity and enzyme inhibitory properties with molecular docking studies of rumex nepalensis, an endemic medicinal plant. *Journal of Food and Nutrition Research* 2021; **9(3)**, 114-123

[22] A Alviz-Amador, R Galindo-Murillo, R Pineda-Alemán, H Pérez-González, E Rodríguez-Cavallo, R Vivas-Reyes and D Méndez-Cuadro. 4-HNE carbonylation induces conformational changes. *Journal of Molecular Graphics & Modelling* 2019; **86**, 298-307.

[23] DA Case, RC Walker, TE Cheatham, C Simmerling, A Roitberg, KM Merz, R Luo, T Darden, J Wang, RE Duke, DR Roe, S LeGrand, J Swails, D Cerutti, G Monard, C Sagui, J Kaus, R Betz, B Madej, C Lin, …, PA Kollman. *Amber 2016 reference manual*. University of California, San Francisco, 2016.

[24] BR Miller, TD McGee, JM Swails, N Homeyer, H Gohlke and AE Roitberg. MMPBSA.py: An efficient program for end-state free energy calculations. *Journal of Chemical Theory and Computation* 2012; **8(9)**, 3314-3321.

[25] L Danielyan, R Klein, LR Hanson, M Buadze, M Schwab, CH Gleiter and WH Frey. Protective effects of intranasal losartan in the APP/PS1 transgenic mouse model of alzheimer disease. *Rejuvenation Research* 2010; **13(2-3)**, 195-201.

[26] Z Deng, J Jiang, J Wang, D Pan, Y Zhu, H Li, X Zhang, X Liu, Y Xu, Y Li, Y Tang and Alzheimer's Disease Neuroimaging Initiative. Angiotensin receptor blockers are associated with a lower risk of progression from mild cognitive impairment to dementia. *Hypertension* 2022; **79(10)**, 2159-2169.

[27] JM Saavedra. Angiotensin II AT1 receptor blockers as treatments for inflammatory brain disorders. *Clinical Science* 2012; **123(10)**, 567-590.

[28] B Ongali, N Nicolakakis, XK Tong, T Aboulkassim, P Papadopoulos, P Rosa-Neto, C Lecrux, H Imboden and E Hamel. Losartan prevents and rescues cerebrovascular, neuropathological and cognitive deficits. *Neurobiology of Disease* 2014; **68**, 126-136.

[29] N Torika, K Asraf, H Cohen and S Fleisher-Berkovich. Intranasal telmisartan ameliorates brain pathology in familial Alzheimer's disease

mice. *Brain, Behavior and Immunity* 2017; **64**, 80-90.

[30] N Torika, K Asraf, RN Apte and S Fleisher-Berkovich. Candesartan ameliorates brain inflammation associated with Alzheimer's disease. *CNS Neuroscience & Therapeutics* 2018; **24(3)**, 231-242.

[31] E Trofimiuk, P Wielgat and J Braszko. Candesartan relieves age-related cognitive impairment. *Pharmacological Reports* 2018; **70(1)**, 87-92.

[32] AG Elkahloun and JM Saavedra. Candesartan neuroprotection negatively correlates with aging and senescence. *Molecular Neurobiology* 2020; **57(3)**, 1656-1673.

[33] NF Khedr, RH Werida and MA Abo-Saif. Candesartan protects against d-galactose-induced neurotoxicity. *Toxicology and Applied Pharmacology* 2022; **435**, 115827.

[34] M Adesuyan, YH Jani, D Alsugeir, ECL Cheung, CSL Chui, R Howard, ICK Wong and R Brauer. Antihypertensive agents and incident alzheimer's disease: A systematic review and meta-analysis of observational studies. *The Journal of Prevention of Alzheimer's Disease* 2022; **9(4)**, 715-724.

[35] TJ Oscanoa, J Amado, X Vidal and R Romero-Ortuno. Angiotensin-receptor blockers and the risk of Alzheimer´s disease: A meta-analysis. *Current Reviews in Clinical and Experimental Pharmacology* 2021; **16(1)**, 73-78.

[36] EA Belachew, GM Peterson and WM Bezabhe. Comparative effects of angiotensin II stimulating and inhibiting antihypertensives on dementia risk: A systematic review and meta-analysis. *Geroscience* 2025; **47**, 5525–5541.

[37] H Zhang, H Unal, C Gati, GW Han, W Liu, NA Zatsepin, D James, D Wang, G Nelson, U Weierstall, MR Sawaya, Q Xu, M Messerschmidt, GJ Williams, S Boutet, OM Yefanov, TA White, C Wang, A Ishchenko, KC Tirupula, R Desnoyer, J Coe, CE Conrad, P Fromme, RC Stevens, V Katritch, SS Karnik and V Cherezov. Structure of the angiotensin receptor revealed by serial femtosecond crystallography. *Cell* 2015; **161(4)**, 833-844.

[38] T Takezako, H Unal, SS Karnik and K Node. Current topics in angiotensin II type 1 receptor research: Focus on inverse agonism, receptor dimerization and biased agonism. *Pharmacological Research* 2017; **123**, 40-50.

[39] H Zhang, H Unal, R Desnoyer, GW Han, N Patel, V Katritch, SS Karnik, V Cherezov and RC Stevens. Structural basis for ligand recognition and functional selectivity at angiotensin receptor. *The Journal of Biological Chemistry* 2015; **290(49)**, 29127-29139.

[40] T Takezako, H Unal, SS Karnik and K Node. Structure-function basis of attenuated inverse agonism of angiotensin II type 1 receptor blockers. *Molecular Pharmacology* 2015; **88(3)**, 488-501.

[41] H Zhang, GW Han, A Batyuk, A Ishchenko, KL White, N Patel, A Sadybekov, B Zamlynny, MT Rudd, K Hollenstein, A Tolstikova, TA White, MS Hunter, U Weierstall, W Liu, K Babaoglu, EL Moore, RD Katz, JM Shipman, M Garcia-Calvo, S Sharma, P Sheth, SM Soisson, RC Stevens, V Katritch and V Cherezov. Structural basis for selectivity and diversity in angiotensin II receptors. *Nature* 2017; **544(7650)**, 327-332.

[42] H Zhang, A Luginina, A Mishin, M Baidya, AK Shukla and V Cherezov. Structural insights into ligand recognition and activation of angiotensin receptors. *Trends in Pharmacological Sciences* 2021; **42(7)**, 577-587.

[43] UM Steckelings, RE Widdop, ED Sturrock, L Lubbe, T Hussain, E Kaschina, T Unger, A Hallberg, RM Carey and C Sumners. The angiotensin AT2 receptor: From a binding site to a novel therapeutic target. *Pharmacological Reviews* 2022; **74(4)**, 1051-1135.

[44] NJ Deng, W Dai and RM Levy. How kinetics within the unfolded state affects protein folding. *The Journal of Physical Chemistry B* 2013; **117(42)**, 12787-12799.

[45] KD Singh, H Unal, R Desnoyer and SS Karnik. Divergent spatiotemporal interaction of angiotensin receptor blocking drugs with angiotensin type 1 receptor. *Journal of Chemical Information and Modeling* 2018; **58(1)**, 182-193.

[46] Y Lobanov, NS Bogatyreva and OV Galzitskaya. Radius of gyration is an indicator of compactness of protein structure. *Molekuliarnaia Biologiia* 2008; **42(4)**,701-706.

Supplementary Material

Table S1 AT1 receptors identified in Uniprot.

SOURCE	IDENTIFIER	METHOD	RESOLUTION	CHAIN	POSITIONS
PDB	4YAY	X-ray	2.90 Å	A	2-319
PDB	4ZUD	X-ray	2.80 Å	A	2-315
PDB	6DO1	X-ray	2.90 Å	A/B	2-319
PDB	6OS0	X-ray	2.90 Å	A	2-319
PDB	6OS1	X-ray	2.79 Å	A	2-319
PDB	6OS2	X-ray	2.70 Å	A	2-319

4YAY | pdb_00004yay (XFEL structure of human Angiotensin Receptor)

Experimental Data Snapshot

Method: X-RAY DIFFRACTION
Resolution: 2.90 Å
R-Value Free:
0.274 (Depositor), 0.316 (DCC)
R-Value Work:
0.228 (Depositor), 0.260 (DCC)
R-Value Observed:
0.231 (Depositor)

Starting Model: other
View more details

wwPDB Validation 3D Report | Full Report

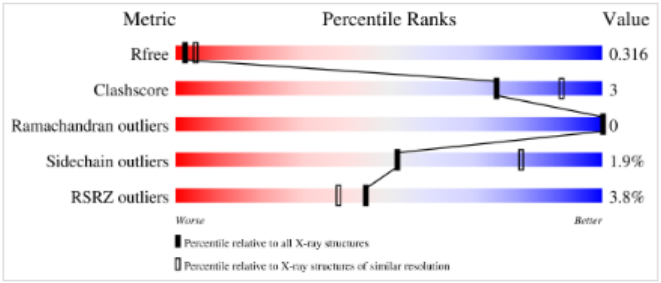

Ligand Structure Quality Assessment

4ZUD | pdb_00004zud (Crystal Structure of Human Angiotensin Receptor in Complex with Inverse Agonist Olmesartan at 2.8A resolution)

Experimental Data Snapshot

Method: X-RAY DIFFRACTION
Resolution: 2.80 Å
R-Value Free:
0.234 (Depositor), 0.240 (DCC)
R-Value Work:
0.194 (Depositor), 0.200 (DCC)
R-Value Observed:
0.196 (Depositor)

Starting Model: experimental
View more details

wwPDB Validation 3D Report Full Report

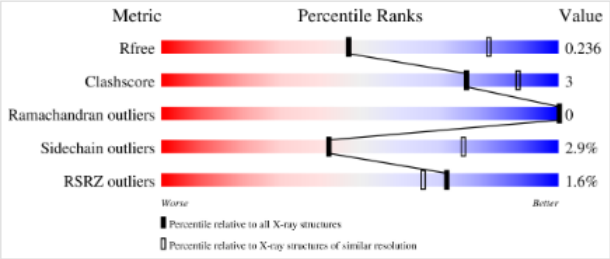

Ligand Structure Quality Assessment

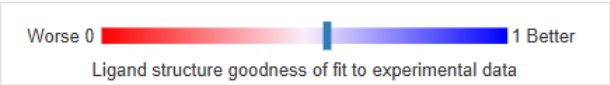

6DO1 | pdb_00006do1 (Structure of nanobody-stabilized angiotensin II type 1 receptor bound to S1I8)

Experimental Data Snapshot

Method: X-RAY DIFFRACTION
Resolution: 2.90 Å
R-Value Free:
0.359 (Depositor), 0.310 (DCC)
R-Value Work:
0.304 (Depositor), 0.310 (DCC)
R-Value Observed:
0.308 (Depositor)

Starting Models: experimental
View more details

wwPDB Validation 3D Report Full Report

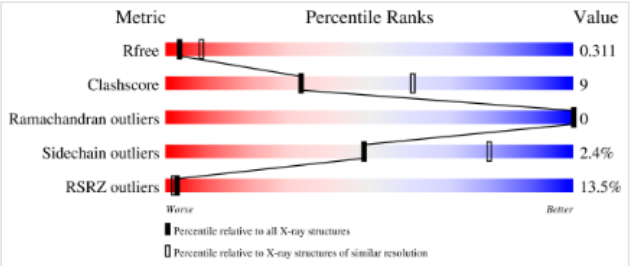

Ligand Structure Quality Assessment

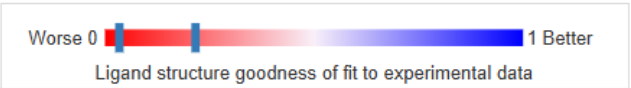

6OS0 | pdb_00006os0 (Structure of synthetic nanobody-stabilized angiotensin II type 1 receptor bound to angiotensin II)

Experimental Data Snapshot

Method: X-RAY DIFFRACTION
Resolution: 2.90 Å
R-Value Free:
0.318 (Depositor)
R-Value Work:
0.259 (Depositor)
R-Value Observed:
0.265 (Depositor)

Starting Model: experimental
View more details

wwPDB Validation 3D Report Full Report

Currently 6OS0 does not have a validation slider image.

6OS1 | pdb_00006os1 (Structure of synthetic nanobody-stabilized angiotensin II type 1 receptor bound to TRV023)

Experimental Data Snapshot

Method: X-RAY DIFFRACTION
Resolution: 2.79 Å
R-Value Free:
0.282 (Depositor), 0.280 (DCC)
R-Value Work:
0.239 (Depositor), 0.240 (DCC)
R-Value Observed:
0.241 (Depositor)

Starting Model: experimental
View more details

wwPDB Validation 3D Report Full Report

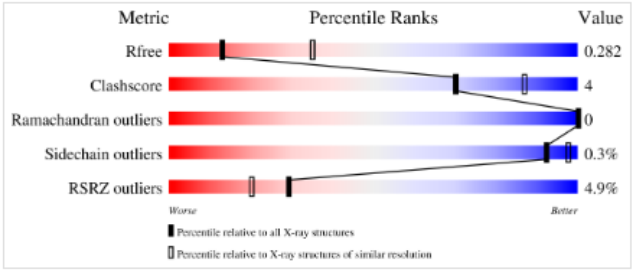

Ligand Structure Quality Assessment

6OS2 | pdb_00006os2 (Structure of synthetic nanobody-stabilized angiotensin II type 1 receptor bound to TRV026)

Experimental Data Snapshot

Method: X-RAY DIFFRACTION
Resolution: 2.70 Å
R-Value Free:
0.285 (Depositor), 0.290 (DCC)
R-Value Work:
0.233 (Depositor), 0.230 (DCC)
R-Value Observed:
0.238 (Depositor)

Starting Model: experimental
View more details

wwPDB Validation 3D Report Full Report

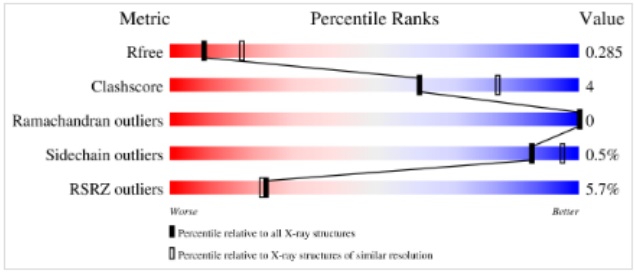

Ligand Structure Quality Assessment

Table S2 AT2 receptors identified in Uniprot.

SOURCE	IDENTIFIER	METHOD	RESOLUTION	CHAIN	POSITIONS
PDB	5UNF	X-ray	2.80 Å	A/B	35-335
PDB	5UNG	X-ray	2.80 Å	B	35-335
PDB	5UNH	X-ray	2.90 Å	A/B	35-335
PDB	5XJM	X-ray	3.20 Å		
PDB	6JOD	X-ray	3.20 Å	A	35-346
PDB	7C6A	X-ray	3.40 Å		
PDB	7JNI	X-ray	3.00 Å	A/B	35-335

5UNF | pdb_00005unf (XFEL structure of human angiotensin II type 2 receptor (Monoclinic form) in complex with compound 1 (N-benzyl-N-(2-ethyl-4-oxo-3-{[2'-(2H-tetrazol-5-yl)[1,1'-biphenyl]-4-yl])

Experimental Data Snapshot

Method: X-RAY DIFFRACTION
Resolution: 2.80 Å
R-Value Free:
0.256 (Depositor), 0.280 (DCC)
R-Value Work:
0.227 (Depositor), 0.250 (DCC)
R-Value Observed:
0.228 (Depositor)

Starting Models: experimental
View more details

wwPDB Validation 3D Report | Full Report

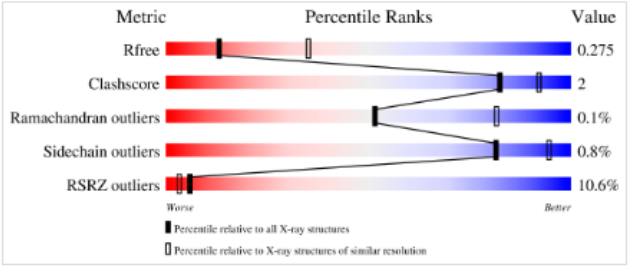

Ligand Structure Quality Assessment

5UNG | pdb_00005ung (XFEL structure of human angiotensin II type 2 receptor (Orthorhombic form) in complex with compound 1 (N-benzyl-N-(2-ethyl-4-oxo-3-{[2'-(2H-tetrazol-5-yl)[1,1'-biphenyl]-4-yl] methyl}-3,4-dihydroquinazolin-6-yl)thiophene-2-carboxamide)

Experimental Data Snapshot

Method: X-RAY DIFFRACTION
Resolution: 2.80 Å
R-Value Free:
0.262 (Depositor), 0.260 (DCC)
R-Value Work:
0.241 (Depositor), 0.260 (DCC)
R-Value Observed:
0.242 (Depositor)

Starting Models: experimental
View more details

wwPDB Validation 3D Report Full Report

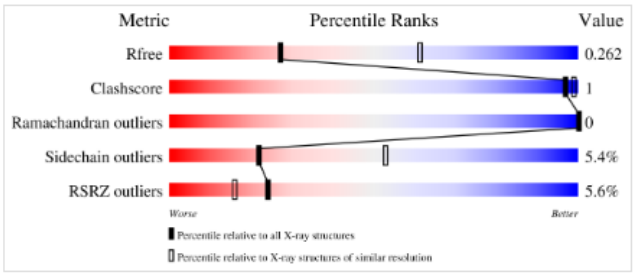

Ligand Structure Quality Assessment

5UNH | pdb_00005unh (Synchrotron structure of human angiotensin II type 2 receptor in complex with compound 2 (N-[(furan-2-yl)methyl]-N-(4-oxo-2-propyl-3-{[2'-(2H-tetrazol-5-yl)[1,1'- biphenyl]-4-yl]methyl}-3,4-dihydroquinazolin-6-yl)benzamide)

Experimental Data Snapshot

Method: X-RAY DIFFRACTION
Resolution: 2.90 Å
R-Value Free:
0.259 (Depositor), 0.300 (DCC)
R-Value Work:
0.216 (Depositor), 0.240 (DCC)
R-Value Observed:
0.218 (Depositor)

Starting Models: experimental
View more details

wwPDB Validation 3D Report Full Report

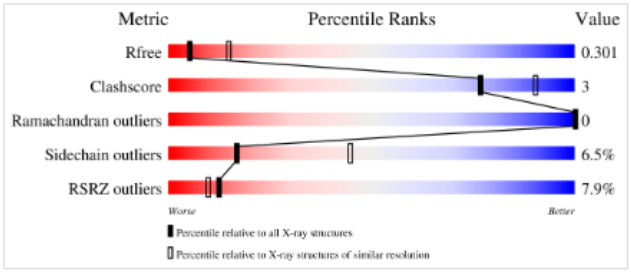

Ligand Structure Quality Assessment

5XJM | pdb_00005xjm (Complex structure of angiotensin II type 2 receptor with Fab)

Experimental Data Snapshot

Method: X-RAY DIFFRACTION
Resolution: 3.20 Å
R-Value Free:
0.275 (Depositor), 0.280 (DCC)
R-Value Work:
0.226 (Depositor), 0.230 (DCC)
R-Value Observed:
0.230 (Depositor)

Starting Models: experimental
View more details

wwPDB Validation 3D Report Full Report

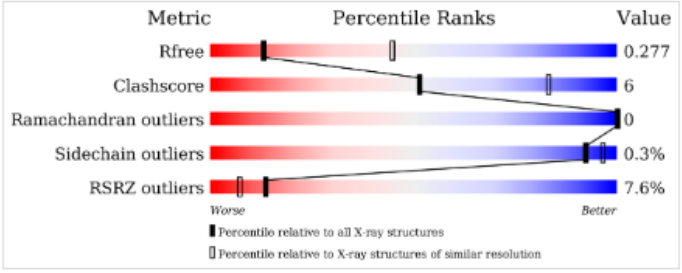

6JOD | pdb_00006jod (Angiotensin II type 2 receptor with ligand)

Experimental Data Snapshot

Method: X-RAY DIFFRACTION
Resolution: 3.20 Å
R-Value Free:
0.287 (Depositor), 0.290 (DCC)
R-Value Work:
0.235 (Depositor), 0.240 (DCC)
R-Value Observed:
0.237 (Depositor)

Starting Models: experimental

wwPDB Validation 3D Report Full Report

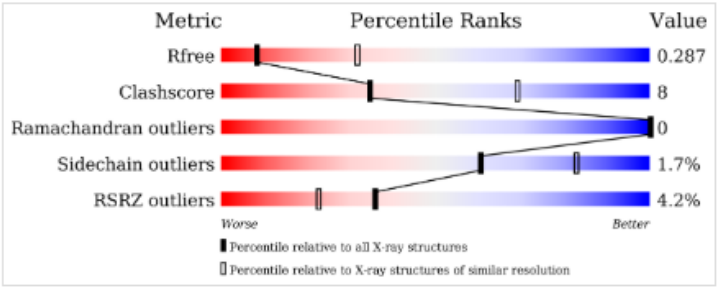

7C6A | pdb_00007c6a (Crystal structure of AT2R-BRIL and SRP2070_Fab complex)

Experimental Data Snapshot

Method: X-RAY DIFFRACTION
Resolution: 3.40 Å
R-Value Free:
0.285 (Depositor), 0.280 (DCC)
R-Value Work:
0.235 (Depositor), 0.230 (DCC)
R-Value Observed:
0.238 (Depositor)

Starting Model: experimental

wwPDB Validation 3D Report Full Report

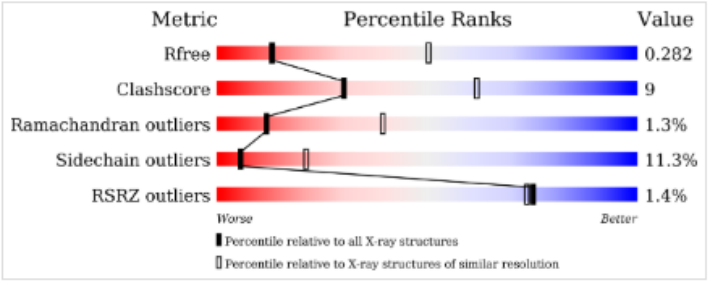

7JNI | pdb_00007jni (Crystal structure of the angiotensin II type 2 receptoror (AT2R) in complex with EMA401)

Experimental Data Snapshot

Method: X-RAY DIFFRACTION
Resolution: 3.00 Å
R-Value Free:
0.273 (Depositor), 0.280 (DCC)
R-Value Work:
0.234 (Depositor), 0.240 (DCC)
R-Value Observed:
0.236 (Depositor)

Starting Model: experimental
View more details

wwPDB Validation 3D Report Full Report

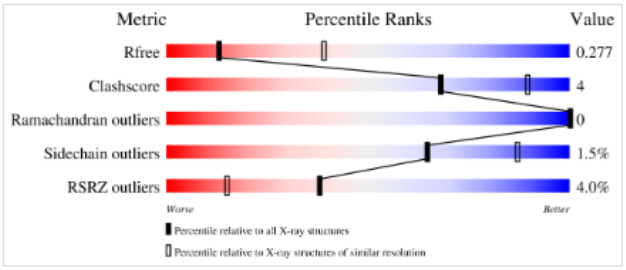

Ligand Structure Quality Assessment

Interpretation of Ramachandran Plots - 5UNF

1) StdMapType3DGeneral

This image represents a general 3D Ramachandran plot. The φ and ψ axes denote torsional angles in degrees, while the Z-axis (frequency) indicates the number of residues adopting each φ/ψ combination. Regions of high frequency (in yellow/green) reflect conformational hotspots typically associated with stable secondary structures such as α-helices (~φ = −60°, ψ = −40°) and β-sheets (~φ = −135°, ψ = 135°). Blue contour lines highlight statistically favored regions.

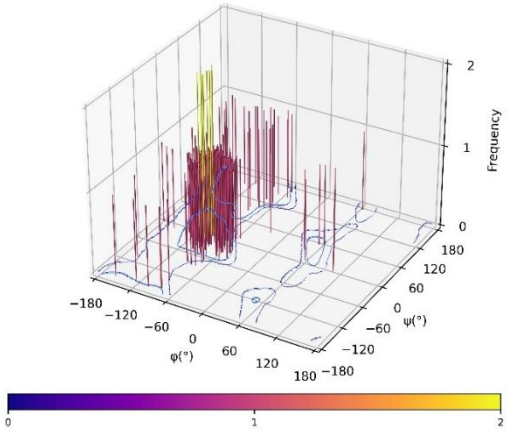

Figure S1 Standard 3D Ramachandran plot 5UNF.

2) StdMapType2DGeneralGly

This 2D plot combines general residues and glycine (Gly). Glycine, lacking a bulky side chain, exhibits greater conformational freedom, hence its distribution appears more scattered. Cyan dots represent glycine, while red and blue dots indicate other residues, potentially outliers. Blue contours delineate allowed regions based on structural databases.

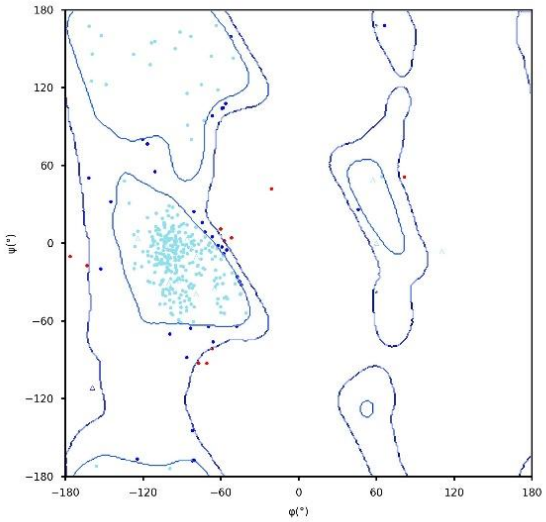

Figure S2 Standard 2D Ramachandran Plot 5UNF.

3) MapType3Dall

This image shows six separate 3D Ramachandran plots based on residue type:
- General: Residues other than glycine or proline.
- Gly: demonstrates broader conformational space.
- Val/Ile: Show restricted areas due to bulky side chains.
- prePro, transPro, cisPro: Represent residues before proline or proline in different isomers.

In all cases, high-frequency regions indicate energetically favorable conformations.

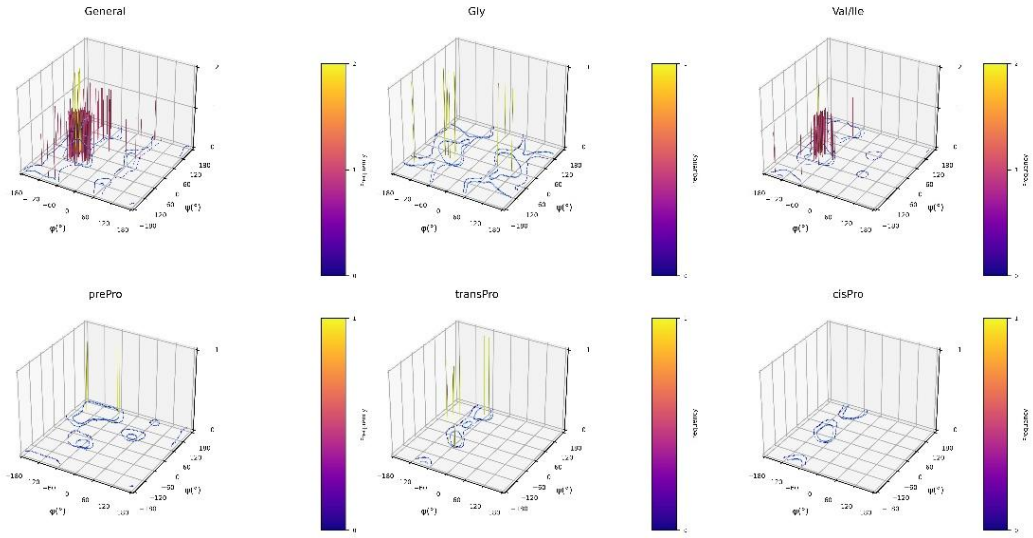

Figure S3 3D Ramachandran plot of six distinct categories of 5UNF: (a) general case (Ala and remaining 15 amino acids), (b) Gly, (c) Val/Ile, (d) pre-Pro, (e) trans-Pro & (f) cis-Pro.

4) MapType2Dall

These are the 2D equivalents of the previous maps, categorized by residue type. They provide a clearer view of residue density (cyan dots) and allowed conformational regions (blue contours). Glycine shows a wide range of conformations, whereas Val/Ile and proline-related residues are much more constrained.

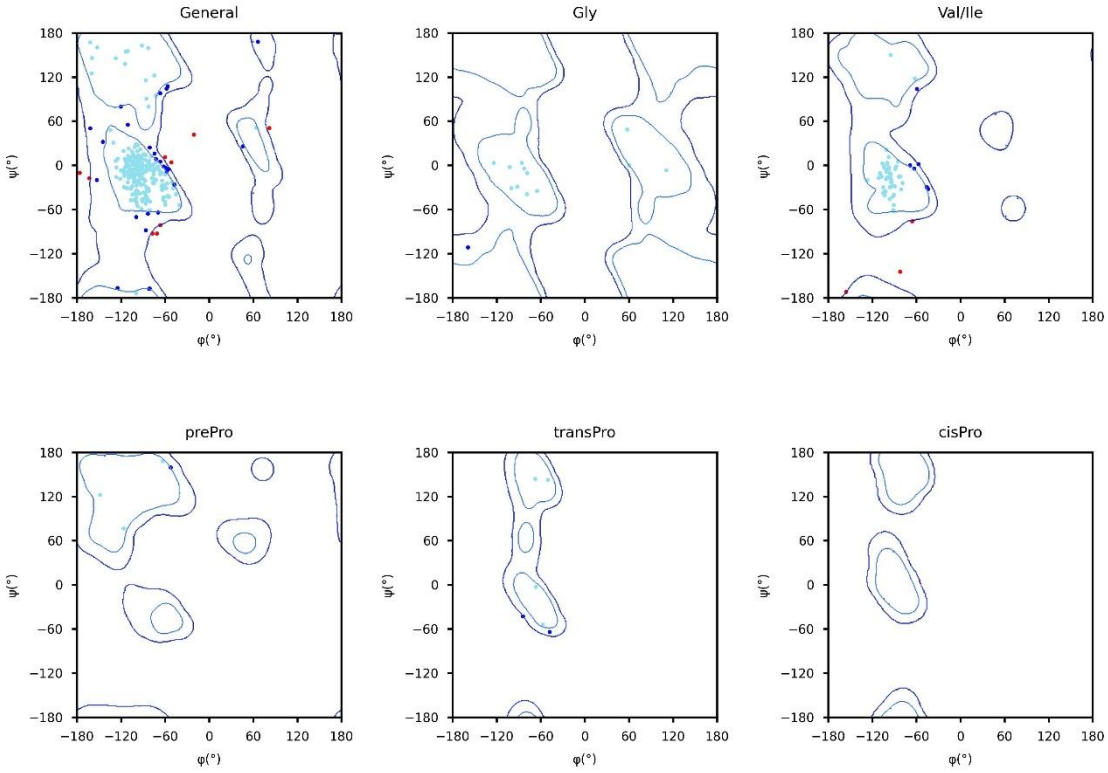

Figure S4 2D Ramachandran plot of six distinct categories of 5UNF: (a) general case (Ala and remaining 15 amino acids), (b) Gly, (c) Val/Ile, (d) pre-Pro, (e) trans-Pro & (f) cis-Pro.

Interpretation of Ramachandran Plots - 4ZUD

1) StdMapType3DGeneral

This 3D Ramachandran plot depicts the general φ/ψ distribution for residues excluding glycine and proline. The frequency axis now reaches a peak of 3, indicating a higher concentration of residues in favored regions. The main conformational clusters are centered around φ ≈ −60° and ψ ≈ −40° (α-helix) and φ ≈ −135°, ψ ≈ 135° (β-sheet). These clusters are denoted by taller bars in yellow and green. Blue contours indicate statistically significantly allowed regions.

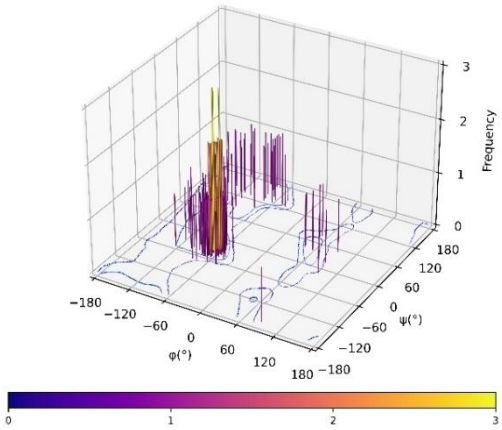

Figure S5 Standard 3D Ramachandran plot of 4ZUD.

2) StdMapType2DGeneralGly

This 2D plot overlays general residues with glycine. Glycine, lacking a side chain, displays greater conformational freedom, resulting in a broader distribution across the φ/ψ map. Most general residues concentrate within the expected α-helical region. Blue contours indicate allowed regions for each residue type. Cyan points correspond to glycine, and blue dots represent other residues.

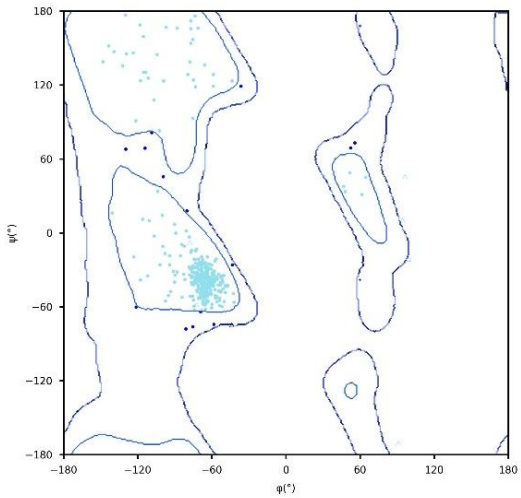

Figure S6 Standard 2D Ramachandran Plot of 4ZUD.

3) MapType3Dall

This panel displays 3D Ramachandran plots categorized by residue type:

- General: Predominant cluster in α-helix region with frequency peaks up to 3.
- Gly: multiple conformational clusters due to high flexibility.
- Val/Ile: Tighter clustering due to steric hindrance from branched side chains.
- prePro, transPro, cisPro: Conformations are limited; proline imposes constraints on backbone angles.

Each map illustrates frequency peaks with colored bars and contour regions showing statistically permitted conformations.

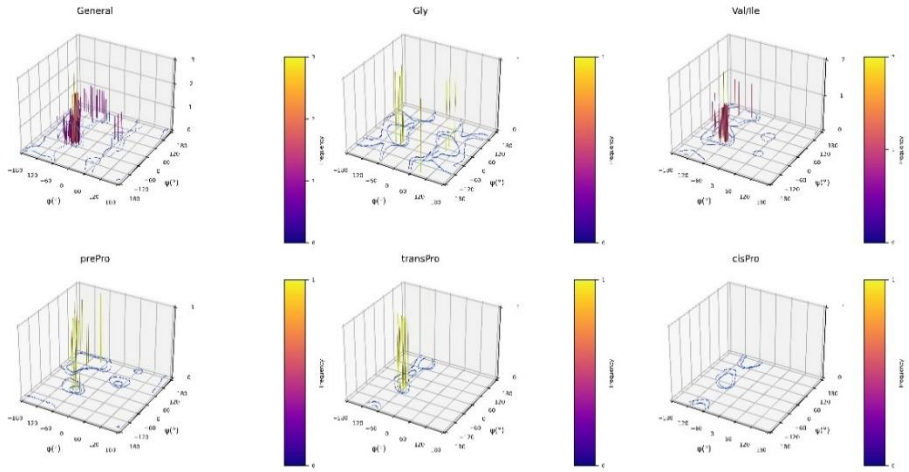

Figure S7 3D Ramachandran plot of six distinct categories of 4ZUD: (a) general case (Ala and remaining 15 amino acids), (b) Gly, (c) Val/Ile, (d) pre-Pro, (e) trans-Pro & (f) cis-Pro.

4) MapType2Dall

The 2D plots highlight the allowed φ/ψ space for various residue types. Glycine's distribution spans multiple regions, while Val/Ile residues are constrained. prePro and proline isomers (trans and cis) exhibit restricted angular distributions, confirming their structural rigidity. Blue contours mark regions validated through structural databases as permissible.

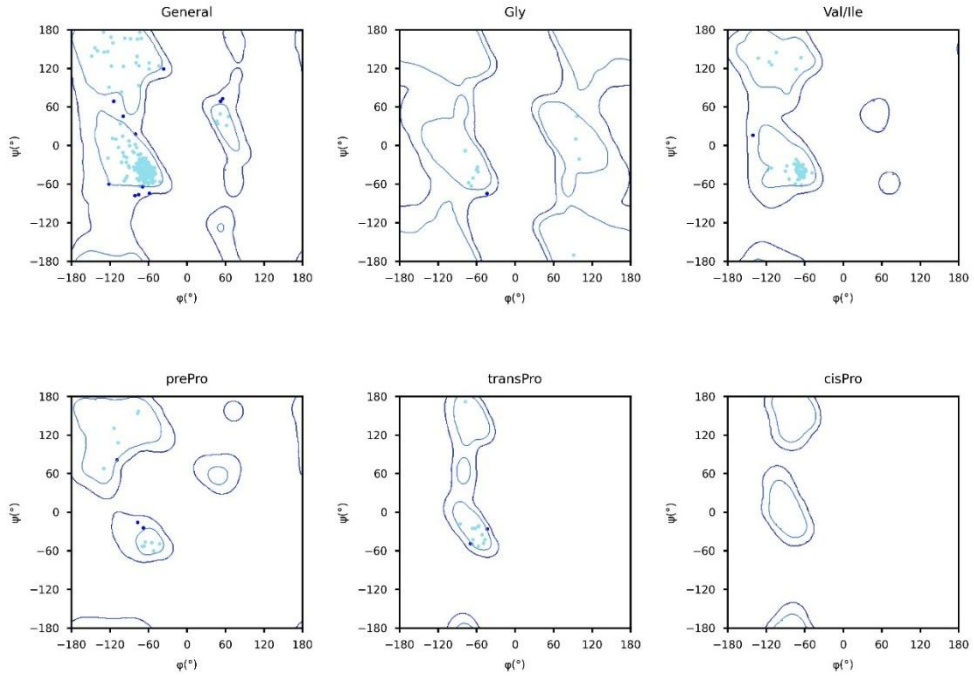

Figure S8 2D Ramachandran plot of six distinct categories of 4ZUD: (a) general case (Ala and remaining 15 amino acids), (b) Gly, (c) Val/Ile, (d) pre-Pro, (e) trans-Pro & (f) cis-Pro.

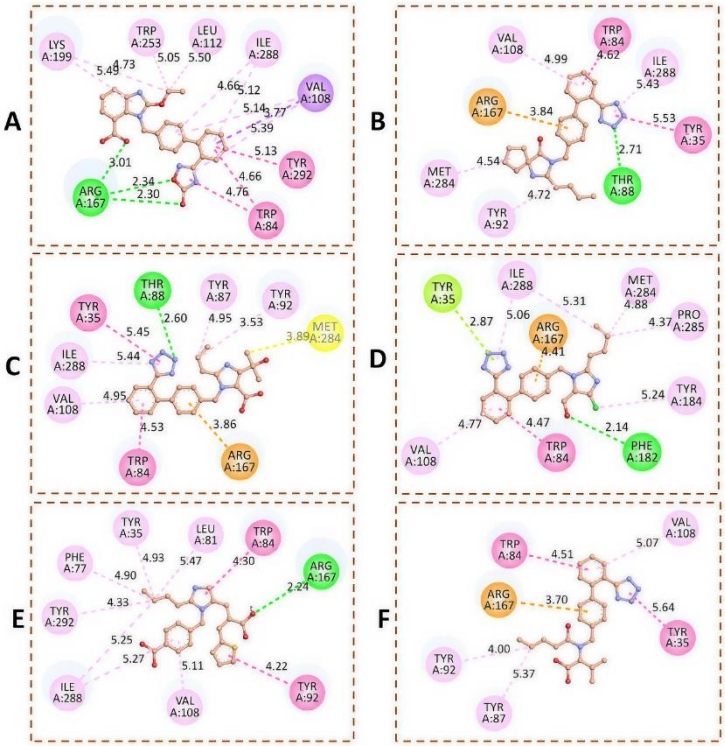

Figure S9 Interactions of ARB and AT1 receptor. (A) Azilsartan; (B) Ibersartan; (C) Olmesartan; (D) Losartan; (E) Eprosartan; (F) Valsartan.

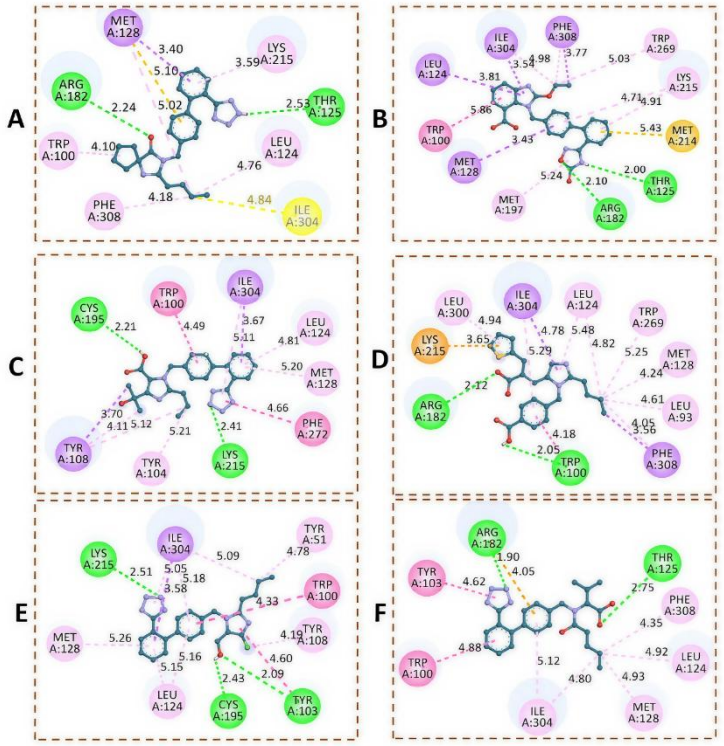

Figure S10 Interactions of ARB and AT2 receptor. (A) Ibersartan; (B) Azilsartan; (C) Olmesartan; (D) Eprosartan; (E) Losartan; (F) Valsartan.